PRZEGLĄD ELEKTROTECHNICZNY

OPEN ACCESS

Arkadiusz MIASKOWSKI
ORCID: 0000-0001-9110-5032
DOI: 10.15199/48.2025.11.36

Temperature analysis in prostate tumor during radiofrequency ablation

Analiza rozkładu temperatury w raku prostaty podczas ablacji z zastosowaniem częstotliwości radiowych

dr hab. inż. Arkadiusz Miaskowski, Lublin University of Technology, Department of Electrical Engineering and Computer Science, Nadbystrzycka 38D, 20-618 Lublin, e-mail: a.miaskowski@pollub.pl

Correspondence address: a.miaskowski@pollub.pl

Abstract: The purpose of this study is to analyze the temperature distribution in the prostate tumor during radiofrequency ablation using computer simulation. Based on the magnetic resonance technique, T2 images were obtained from the patient and three-dimensional anatomically correct models of the prostate and tumor were prepared. A needle-type bipolar electrode model was created as a source of radiofrequency energy that is converted to temperature. The electrode was then inserted into the tumor, and the temperature distributions were analyzed for different values of electrical potential applied to the electrode. In addition to temperature and electromagnetic field, cumulative equivalent minutes at 43 oC were considered as a factor of thermal dose effect.

Keywords: computer simulation, radiofrequency ablation, prostate cancer

Streszczenie: Celem niniejszej pracy jest analiza rozkładu temperatury w guzie prostaty podczas ablacji o częstotliwości radiowej z wykorzystaniem symulacji komputerowej. W oparciu o technikę rezonansu magnetycznego, uzyskano obrazy T2 od pacjenta i przygotowano trójwymiarowe, anatomicznie poprawne, modele prostaty i guza. Stworzono model dwubiegunowej elektrody typu igłowego jako źródła energii o częstotliwości radiowej, która jest przekształcana w temperaturę. Elektroda została następnie wprowadzona do guza, a rozkłady temperatury zostały przeanalizowane dla różnych wartości potencjału elektrycznego przyłożonego do elektrody. Oprócz temperatury i pola elektromagnetycznego, jako czynnik efektu dawki termicznej uwzględniono skumulowane równoważne minuty w temperaturze 43 oC.

Słowa kluczowe: symulacja komputerowa, ablacja z zastosowaniem częstotliwości radiowych, rak prostaty

Introduction

Prostate cancer is one of the major oncological problems in men and current treatment methods such as radiotherapy and hormonal therapy often do not provide optimal therapeutic results. It is the second most common cancer diagnosis in men and the fifth leading cause of death worldwide [1]. The disease may be asymptomatic in the early stages and often requires only active surveillance. According to GLOBOCAN 2018, 1,276,106 new cases of prostate cancer were reported in 2018 with a higher incidence in developed countries, which results from differences in the availability of diagnostics. Morbidity and mortality increase with age, reaching the highest values in men over 65 years of age [2-5]. Diagnosis of prostate cancer and assessment of its stage are key in clinical care. The basis of diagnosis remains a rectal examination and determination of PSA level in blood as well as multiparametric magnetic resonance imaging (mpMRI) for the assessment of local advancement. The gold standard for diagnosis is TRUS biopsy [6-7]. Unfortunately, advanced disease is characterized by a high mortality due to tumor heterogeneity at the genetic and biological level, which makes it difficult to obtain durable therapeutic responses [8]. In the early 21st century, androgen deprivation therapy was developed for metastatic disease and in the last decade, six new systemic drugs have been approved for the treatment of castration-resistant cancer [9]. Unfortunately, all of these methods are associated with side effects, such as erectile dysfunction, decreased libido, obesity, or bone loss [10].

Radiofrequency ablation (RFA) is one of the most commonly employed thermal ablation techniques. It uses radiofrequency energy to generate heat, which destroys cancer cells. During the RFA procedure, an electrode is inserted directly into the tumor, usually percutaneously under image guidance. Radiofrequency current flowing through the electrode heats the tissue to a temperature of 60-100°C, which leads to protein denaturation and coagulative necrosis [11,12]. Thermal ablation is a minimally invasive method of treating cancer, which involves destroying cancer cells using high temperature. It is mainly used in cases where the traditional surgery is too risky or impossible. This method has found particular application in the treatment of liver tumors [13], but it is also used to treat kidney tumors [14], lung cancers [15], thyroid cancers [16], soft tissue and bone sarcomas [17], adrenal tumors [18], as well as prostate cancer [19].

Materials and methods

To present the problem of temperature distribution during FR ablation in the most realistic way, the analysis was performed based on T2 magnetic resonance images. The patient was diagnosed with prostate cancer as depicted in Fig. 1. The volume of prostate gland was 48990.9 mm^3, while the tumor volume was 5937.55 mm^3. The tumor was classified to the five categories of the PI-RADS rate and was spreading from the base, through the middle part toward the apex as shown schematically in Fig. 2.

As a source of heat the bipolar RF electrode model was prepared. The model was based on the electrode for electrosurgical device as shown in Fig. 3. In this case the electrode tip had a ratio of 5:2:8 for cathode (C), connecting portion of dielectric (D), and anode (A), respectively.

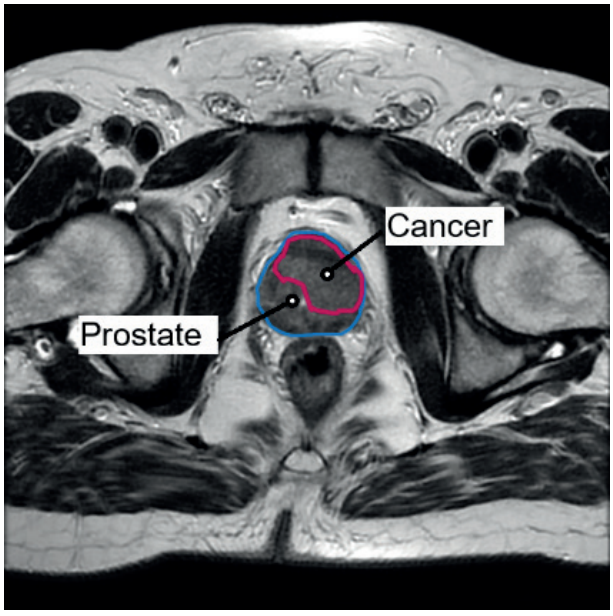

Fig. 1. T2 MRI slice with cancer and prostate highlighted

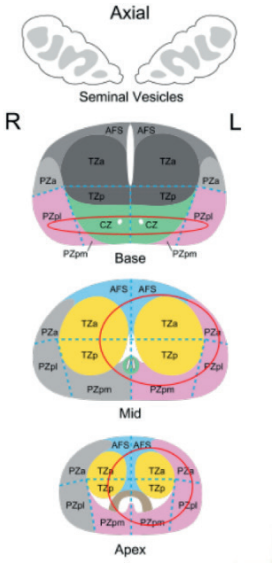

Fig. 2. Tumor location (marked red) with regard to prostate

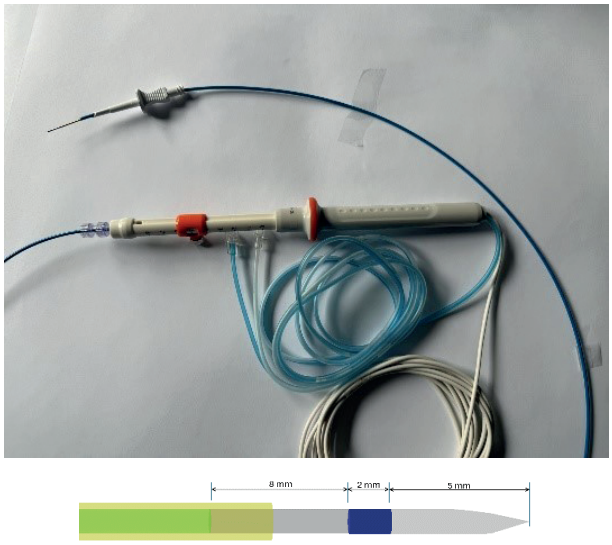

Fig. 3. Photo of the electrode for the electrosurgical device used in this study, along with the dimensions of the electrode tip

The simulations were conducted using Sim4Life software under academic license (Sim4Life, www.sim4life.swiss). First, the Electro Quasi-Static solver was applied to analyze electromagnetic field, and then the transient thermal solver for modelling of heat energy.

Mathematical model

To numerically investigate temperature distribution in the model a various approaches can be applied like, for example, a coupled problem [20] but in this paper a multi-step approach was used [21, 22]. First,

the electro quasi-static approximation was applied to calculate the electric field. Second, the temperature distribution was obtained on the base of Pennes bioheat equation [23]. In case of the first step, without source current the vector potential vanishes and therefore the electric field depends only on the scalar potential ϕ. To satisfy the potential continuity one can define the problem as follows:

$$\nabla \cdot \tilde{\epsilon} \nabla \phi = 0 \tag{1}$$

where
$\tilde{\epsilon} = \epsilon_r \epsilon_0 + \sigma/(j\omega)$ – is the complex permittivity,
σ – is the electric conductivity,
$j^2 = -1$, $\omega = 2\pi f$ where f is the frequency.
Finally, the electric field, **E**, can be expressed as follows [24]:

$$\mathbf{E} = -\nabla \phi \tag{2}$$

On this basis one can calculate the electric loss density (p) defined as the product of the local specific absorption rate (SAR) and the density (ρ) as:

$$p = \rho SAR = \sigma \frac{|\mathbf{E}|^2}{2} \tag{3}$$

where $|\mathbf{E}|^2$ denotes the square magnitude of the electric field.

In the case of step two, the electric loss density, p, obtained in the first step, was used in the bioheat equation as follows:

$$\rho c \frac{\partial T}{\partial t} = \nabla (\kappa \nabla T) + \rho Q + \rho SAR - \rho_b c_b \rho \omega (T - T_b) \tag{4}$$

where:
c – is the specific heat,
κ – is the thermal conductivity,
ω – is the perfusion rate, and subscript b denotes blood parameters like density (ρ_b), temperature (T_b) and specific heat (c_b),
Q – denotes the specific metabolic heat generation rate.
Besides, Neumann boundary conditions i.e. thermal isolation, were set to prevent thermal spread toward other tissues.

The schematic drawing of the aforementioned model is shown in Fig. 4, where subdomain Ω_1 indicates the phantom, subdomain Ω_2 prostate and subdomain Ω_3 tumor. In the case of electro quasi-static approximation Dirichlet boundary conditions $d\Omega$ were used, while in the transient thermal solver Neumann boundary conditions, $\frac{\partial \Omega}{\partial n}$, were assigned to the phantom (without $\partial\Omega$).

To assess the exposure to a heat source, such as medical ablation instruments, cumulative equivalent minutes at 43 °C can be used i.e. CEM_{43} [25]. In this

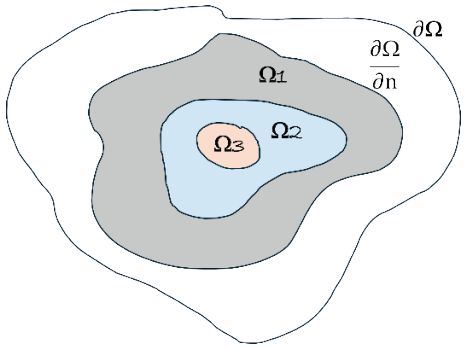

Fig. 4. Boundary conditions used in the model (Ω_1 – phantom, Ω_2 – prostate, Ω_3 – tumor)

way one can specify the amount of heat absorbed by means of a thermal dose. CEM_{43} concept is usually formulated as:

$$\mathrm{CEM}_{43} = \int_0^t R^{43-T(t)} dt$$

where R = 0.5 for T > 43 °C, R = 0.25 for R in the range from 39 to 43 °C, and R = 0 for T < 39 °C.

Dielectric properties

The following dielectric properties calculated for 100 kHz were assigned to each region (see Fig. 4) as collected in Tables 1 and 2:

Table 1. The properties assigned to the model for electro quasi-static solver [26].

Tissue	ε_r	σ S/m
Prostate	5716.9	1045.0
Phantom	101.5	911.0
Tumor	8089.1	1090.0
Dielectric (D)	2.25	0.0005
Electrode (A,C)		---

Table 2. The thermal properties assigned to the model for thermal solver [26].

Tissue	ρ kg/m³	c J/kg/K	κ W/m/K	ω_b ml/kg/min	HGR W/kg
Prostate	1045	3760.0	0.5115	394.1	6.104
Phantom	911	2348.3	0.2114	32.71	0.506
Tumor	1090	3421.2	0.4945	36.74	0.906

HGR – heat generation rate

As for the tumor, the electric and thermal properties of a muscle tissue were assigned, which is a common practice in computational bioelectromagnetic [27, 28].

Results

When taking into account the mathematical model presented in Fig. 4, 3D CAD models of every subdomain including the applicator were prepared. As depicted in Fig. 5, the model of needle-type FR applicator was inserted in the prostate tumor (subdomains Ω_2, Ω_3), which in turn was placed in the phantom (Ω_1) marked with a black square. To measure the effectiveness of the applicator the width and the depth of the area surrounding its tip might be considered (see Fig. 1-right).

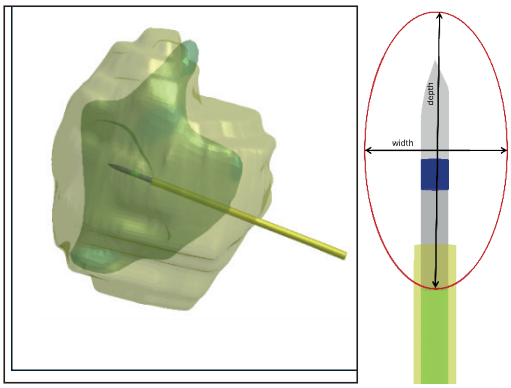

Fig. 5. 3D CAD model of RF applicator inserted in the prostate tumor (left) and the needle-type applicator working area (right).

As it was mentioned before, to analyze electromagnetic field, the Electro Quasi-Static solver was applied. In electromagnetic dosimetry, the quantity that measures the energy deposited in biological tissues is usually denoted as SAR. In Fig. 6, it can be seen the SAR distribution in the model for the potential φ=15V assigned to the cathode. In this case, the maximum SAR, which was obtained, was 51.2 kW/kg (the cross-section through the applicator can be seen in dB scale). One can also see that the cross-section through the tumor is much larger than comparing with the one through SAR pattern. Moreover, the SAR pattern has ellipsoid-like shape with width 11.5 mm and the depth 17 mm.

It is obvious that the power losses produced by the conduction current $\sigma\mathbf{E}$ results in heating of the region. So, in the next step, the temperature distribution was evaluated for initial temperature T_0=37 °C. Fig. 7 shows the temperature distribution after 500 seconds of heating which should be understood as the result of the SAR obtained in the previous step. One may notice that the temperature distribution has also ellipsoid-like shape and maximum is 68.6 °C. As for the width and the depth, they are 10.0 mm and 11.8 mm, respectively.

Finally, for assessment of the inflicted tissue damage under the aforementioned conditions, CEM_{43} parameter was calculated as it is depicted in Fig. 8.

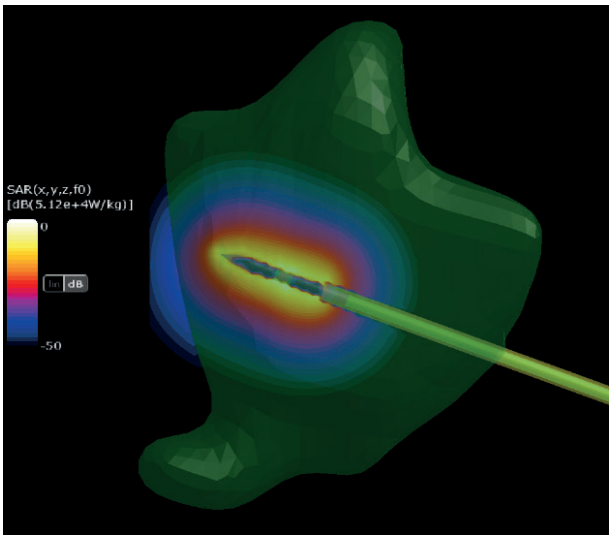

Fig. 6. SAR distribution in dB scale (max value 5.12e+4 W/kg) for φ=15V (blue color indicates temperature 37 °C).

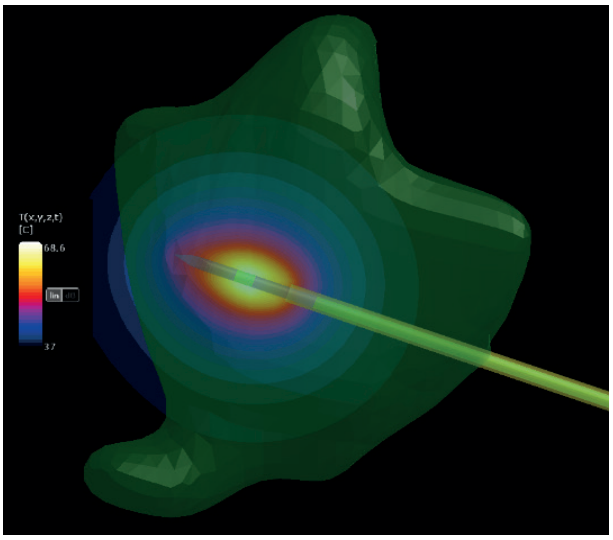

Fig. 7. Temperature distribution after 500 sec. of heating (cross-section through the applicator; blue color indicates temperature 37 °C).

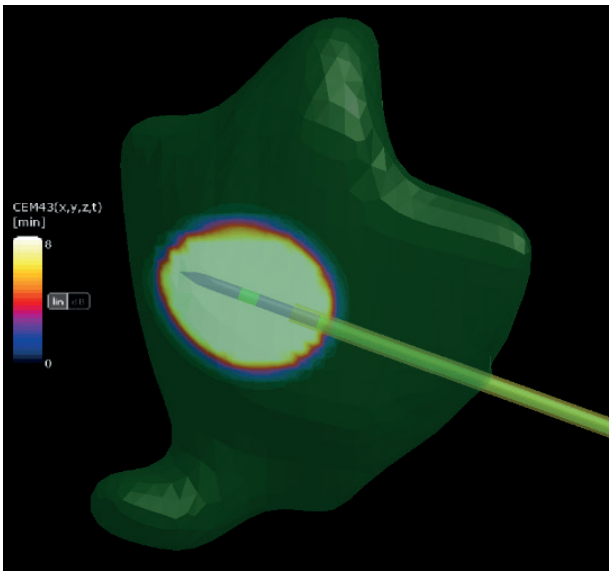

Fig. 8. CEM_{43} distribution – bright region might suffer from thermal damage.

One should realize, that most of the tumor tissue damage will occur in the brightest region of depicted cross-section. In this case, the width is 11.3 mm and the depth is 14.4 mm.

As the last point of the temperature analysis in the prostate tumor the above methodology was prepared for different values of electric potential applied to the cathode i.e. from 10 to 25 V with step 5 V. In Fig. 9, the temporal evaluation of temperature at location D can be seen. Fig. 9 shows both heating (up to 500 sec.) and cooling phases (from 500 up to 600 sec.). When taking into consideration the obtained temperature-time dependencies, it can be concluded that the value of the applied potential should be found in the range from about 15 to 20 V.

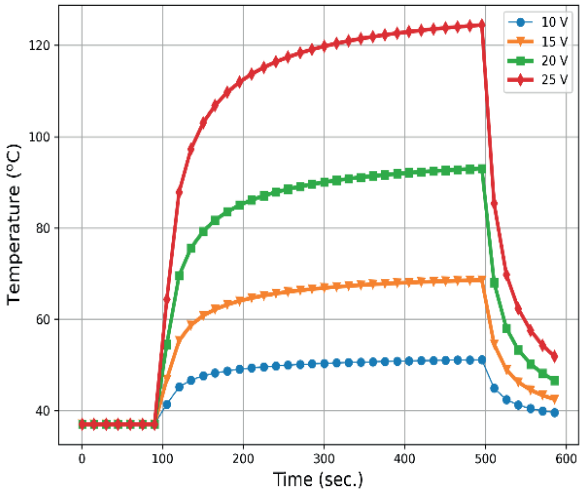

Fig. 9. Temperature over time in the center of applicator.

Conclusions

The paper presents the temperature analysis in the prostate tumor. First, using electro quasi-static approximation the energy carried by the time-harmonic electromagnetic field deposited in prostate tumor was evaluated for different values of the potential. Next, on the basis of bioheat Pennes equation the temperature distribution was investigated. Finally, to evaluate the effectiveness of the applicator CEM_{43} distribution was obtained.

As for EM field, the energy absorbed by the tumor was denoted as the SAR, which provides the ratio between the deposited power density and the mass. In the case of temperature distribution, the effectiveness of needle-type applicator was assessed via two parameters i.e. the width and depth. Besides, one should realize that the Neumann boundary condition could be applied due to the short duration of the heating. When heating takes longer, Robin's boundary conditions should be assumed.

When considering the different shapes of the tumors, it can be concluded that due to their irregular shape, each tumor should be treated separately, and treatment planning should be prepared in detail, as the insertion site, width and depth of working area together with the applied potential can play a key role for RF ablation therapy planning.

Acknowledgments: Heartfelt thanks to Katarzyna Dyndor, Phd, from 1st Military Clinical Hospital with the Outpatient Clinic, Department of Radiology in Lublin, for her help in analyzing the MRI images

Received: 10.11.2025, **Accepted:** 12.11.2025, **Published:** 24.11.2025

REFERENCES

[1] Chatterjee S., et al. Enhancing prostate cancer treatment: Synergistic effects of mechano-thermal focused ultrasound and radiation therapy, Cancer Research, 84 (2024), 709-709.
[2] Pernar C. H., et al., The epidemiology of prostate cancer, Cold Spring Harbor perspectives in medicine, 8 (2018), a030361.
[3] Rawla P., Epidemiology of prostate cancer, World journal of oncology, 10(2019), 63.
[4] Gandaglia, G., et. al., Epidemiology and prevention of prostate cancer. European urology oncology, 4 (2021), 877-892.
[5] Sekhoacha, M., et. al., Prostate cancer review: genetics, diagnosis, treatment options, and alternative approaches. Molecules, 27(2022), 5730.
[6] Descotes L-C. Diagnosis of prostate cancer, Asian journal of urology 6(2019), 129-136.
[7] Catalona, W. J., Prostate cancer screening, Medical Clinics, 102(2018), 199-214.
[8] Wang G. et al., Genetics and biology of prostate cancer, Genes & development 32 (2018), 1105-1140.
[9] Teo, M. Y., et. al., Treatment of advanced prostate cancer, Annual review of medicine, 70(2019), 479-499.
[10] Barani M., et. al., Nanotreatment and nanodiagnosis of prostate cancer: recent updates, Nanomaterials, 10(2020), 1696.
[11] Wu J., et. al, Radiofrequency ablation: mechanisms and clinical applications, MedComm, 5(2024), 746.
[12] Pahade A., et. al., Monitored anesthesia care for percutaneous radiofrequency ablation of oncological lesions: a retrospective analysis and literature review, Anaesthesia, Pain & Intensive Care, 28(2024), 534-540.

[13] Kulig J., et. al., Histopathological specimen of the resected metastatic liver tumor after the RF Ablation, Przegląd Lekarski, 62(2005), 287-291.
[14] Vroomen L. G. P. H., et al., Irreversible electroporation and thermal ablation of tumors in the liver, lung, kidney and bone: What are the differences?, Diagnostic and interventional imaging, 98(2017), 609-617.
[15] Rangamuwa K., et al., Thermal ablation in non-small cell lung cancer: a review of treatment modalities and the evidence for combination with immune checkpoint inhibitors, Translational lung cancer research, 10(2021), 2842.
[16] Cho S. J., et al., Thermal ablation for small papillary thyroid cancer: a systematic review, Thyroid, 29(2019), 1774-1783.
[17] Filippiadis D. K., et al., Percutaneous image-guided ablation of bone and soft tissue tumours: a review of available techniques and protective measures, Insights into imaging, 5(2014), 339-346.
[18] Xie L., et al., Comparison between surgery and thermal ablation for adrenal metastases: a retrospective study, International Journal of Hyperthermia, 38(2021), 1541-1547.
[19] Séguier D., et al., Intratumoural immunotherapy plus focal thermal ablation for localized prostate cancer, Nature Reviews Urology, 21(2024), 290-302.
[20] Gas P., Wyszkowska J., Influence of multi-tine electrode configuration in realistic hepatic RF ablative heating, Archives of Electrical Engineering, 68(2019), 521–533
[21] Sawicki B., Miaskowski A., Numeryczny model hipertermii płynu magnetycznego, Przegląd Elektrotechniczny, 07(2013), p. 86
[22] Sawicki B., Miaskowski A., Nonlinear higher-order transient solver for magnetic fluid hyperthermia, Journal of Computational and Applied Mathematics, 2014, 134-151.
[23] Miaskowski A., Gas P., Numerical Estimation of SAR and Temperature Distributions inside Differently Shaped Female Breast Tumors during Radio-Frequency Ablation, Materials 16(2023), 223-243.
[24] Fotis G., Fotis, G. Electromagnetic Fields Radiated by Electrostatic Discharges: A Review of the Available Approaches. Electronics, 12(2023), 2577
[25] van Rhoon G. C., Is CEM43 still a relevant thermal dose parameter for hyperthermia treatment monitoring? International Journal of Hyperthermia, 32(2016), 50-62.
[26] Baumgartner C, et al., IT'IS Database for thermal and electromagnetic parameters of biological tissues, Version 4, April 06, 2024,DOI:10.13099/VIP21000-04-2. itis.swiss/database
[27] Rahpeima R, Lin C-A., Numerical study of magnetic hyperthermia ablation of breast tumor on an anatomically realistic breast phantom. PLoS ONE, (2022),17(9).
[28] Gas P., Miaskowski A., Dobrowolski D., Przegląd Elektrotechniczny, 02(2020), 146.